
DEGRADATION
OF POLYMERS

Oxidative Ageing and Structural Characterization of Naturally Weathered Low Density Polyethylene Films

N. H. Benmiloud^{a,*}, S. F. Chabira^b, A. H. Bhat^c, Y. K. Dasan^c, and M. Sebaa^d

^a*Mechanics Laboratory (lme)-RFME, Faculty of Technology, Amar Telidji University, Laghouat, 03000 Algérie*

^b*Engineering Process Department, Mechanics Laboratory (lme)-RFME, Faculty of Technology, Amar Telidji University, Laghouat, 03000 Algérie*

^c*Fundamental and Applied Sciences Department, Universiti Teknologi Petronas, Bandar Seri Iskandar, Tronoh Perak, 31750 Malaysia*

^d*Mechanical Engineering Department, Mechanics Laboratory (lme)-RFME, Faculty of Technology, Amar Telidji University, Laghouat, 03000 Algérie*

**e-mail: nh.benmiloud@lagh-univ.dz*

Received November 5, 2019; revised March 8, 2020; accepted March 26, 2020

Abstract—Natural weathering was performed in a Saharan region to characterize its effect on low-density polyethylene (LDPE) films used for greenhouse coverings. The morphological changes, followed by differential scanning calorimetry (DSC), showed that the damages caused by the oxidation of tie molecules increased the lamellae thickness, its distribution and the crystallinity. Wide-angles X-ray diffraction (WAXD) was used to follow both the structural and morphological changes of the film. The WAXD crystallinity increase had the same trend as that determined by DSC. Field emission scanning electron microscopy (FESEM) of the films surfaces and cross-sections showed that the degradability increased with exposure time. Atomic force microscopy (AFM) analysis was used to evaluate changes in the surface morphology and roughness. Ageing caused a change of the surface topography of the LDPE films as observed by the increase of surface roughness which is indicated by the increase of the roughness parameters. Simultaneously the peaks-spacing \bar{d} decreased.

DOI: 10.1134/S1560090420040016

INTRODUCTION

Polyolefins have been widely used owing to their high performance such as high modulus, high tensile stiffness, high chemical resistance and low cost for processing. These materials have numerous applications, such as cable and wire insulation, food packaging, medical components and many more [1]. One of the most weight consumption of this type of material is their use for greenhouses coverings. In such an application, the polyethylene film is subjected to weathering agents such as sunlight, thermal cycles, temperature, humidity, rain, atmospheric oxygen, windblown sand and pollutants [2, 3]. These environmental parameters can affect adversely the polymer's thermal and structural properties. These are due to the microstructural changes undergone by the macromolecular structure, mainly governed by chain scission and cross-linking [4–6].

Knowing that LDPE is a semicrystalline polymer having a glass transition temperature far below ambient temperature, the toughness of the material is controlled by the efficiency of the tie molecules that link neighboring crystallites across the amorphous phase.

The rapid diffusion of oxygen within the disordered amorphous interstices leads to chain scission in the macromolecules activated by consequence of the progressive exhaustion of vinylidenes ($\text{CH}_2=\text{C}<$), (characterizable at 888 cm^{-1} in IR spectra) by reaction with alkyl radicals and provoking the crosslinking of the macromolecules. In parallel, natural weathering causes the continuous production of vinyl groups ($\text{CH}_2=\text{CH}-$), (910 cm^{-1} in IR spectra). They result from chain scission reactions occurring in the proximity of carbonyl groups via the well-known Norrish type II reaction process [2, 4, 7–10]. The consequence of these chemical changes on the material's morphology is an increase of the crystallinity which adversely affects the mechanical properties by making it much more brittle. The structural morphology of polyethylene is an alternation of crystalline and amorphous layers (two-phases system). The oxidation damages are mainly confined in the amorphous phase which is responsible for the cohesiveness of the whole. Also, the damages (chain scissions) caused to the amorphous tie molecules contribute to increasing the crystalline concentration. In a previous study, some of us

and others analyzed the morphological changes undergone by LDPE films exposed outdoors in a Sub-Saharan region (Laghouat, Algeria) [7, 11]. They showed that the short chain segments coming from chain scissions can either contribute in the thickening of the existing crystalline lamellae or in the nucleation of new crystallites in the films. In addition to the morphological alteration, the material underwent surface changes which were symptoms of the photo-oxidation mechanisms responsible for the degradation of the polymer structure. ATR-FTIR, microhardness techniques contributed in the revelation of the heterogeneous alteration of the LDPE films [12]. However, the question arises; in addition to the numerous microstructural, morphological, and mechanical characterizations investigated to understand the ageing effect on the polyethylene films, could the microscopic techniques (atomic force microscopy (AFM) and/or field emission scanning microscopy (FESEM)) visualize the surface alteration undergone by the material?

The aim of this work was to highlight the effect of weathering on the surface topography of the LDPE films weathered in Algerian Sub-Saharan facilities. The region is characterized by an average temperature of 7.8°C in winter, 28.9°C in summer ($T_{\max} = 45^\circ\text{C}$), a rainfall of 176 mm, an average wind speed of 17.2 km/h, and sun radiation which can reach 1100 W/m². The variation of the crystallinity degree was characterized by means of DSC and WAXD. WAXD also allowed identifying the type of crystalline lattice. Field emission scanning microscopy (FESEM) and atomic force microscopy (AFM) were used to visualize the surface topography of the LDPE films upon ageing. Previously, the characterization of polyethylene film surfaces which underwent different types of artificial aging (irradiation, plasma treatment, etc.) showed an irremediable modification of the surface morphology by increasing the roughness [13, 14]. However, we will interest to check the surface topographies and the modification of naturally weathered low density polyethylene films by the AFM and FESEM techniques [14–17].

EXPERIMENTAL

Material and Exposure

The LDPE used in this investigation was a commercial grade supplied by the Saudi Basic Industries Corp (SABIC), Saudi Arabia as “LDPE 2100 T N00W”, ($\rho_s = 0.92 \text{ g/cm}^3$, MFI = 0.33 g/10 min). This polymer was a neat grade, exempt of stabilizing agents. Films were produced by blowing extrusion from the raw material in an Algerian industry (Sofiplast of Sétif). The drawing speed of the production line was fixed to 15 cm/s. The melt was extruded at about 175°C and blown in a continuous process characterized by a bubble diameter of 4.4 m and a wall

thickness of 160 μm . It is known that the properties in the machine direction (MD) depend on the draw down ratio (DDR) and those in the transverse direction (TD) to the blowup ratio (BUR) [18].

The weathering site is located at Laghouat, Algeria (33°48' N 2°52' E) and the exposure time was from December to the following August. The films were mounted on metallic frames, south oriented and inclined by 33° relatively to the horizontal according to the NF51-165 standard. Samples were picked up periodically, during all the ageing period, from film zones sufficiently far away from the contact points with the holding frame. This precaution was taken to avoid uncontrolled overheating of the material. The maximum of eight months of exposure corresponds to the time at which the film became too brittle to resist the wind strength; this corresponds to the limit of the experimental exposure.

Differential Scanning Calorimetry (DSC)

A DSC apparatus (Perkin Elmer TA-Q2000, USA) was used to conduct the thermal analysis of the non-weathered and weathered samples (two, four, six and eight months of exposure). A few milligrams (10 mg) were taken from the films and pressed in an aluminum pan and the whole then placed in the furnace. They were subjected to a thermal cycle: (i) heating from 10 up to 150°C with a heating rate of 10 grad/min, (ii) maintaining the sample at 150°C for a few seconds before being subjected to (iii) progressive cooling with a cooling rate of 10 grad/min down to 10°C. Both the melting and cooling scans were recorded under inert atmosphere (N₂). Indium was used for calibration. The melting temperature was determined as the maximum of the melting peak and the crystallization temperature was the maximum of the re-crystallization peak during cooling. The mass-based degree of crystallinity was calculated with reference to the thermodynamic heat of fusion of 100% crystallized polyethylene ($\Delta H_c = 290 \text{ J/g}$). The specific heats C_p of melting and crystallization were determined from the areas of the fusion and the re-crystallization peaks, respectively [19]. Furthermore, the DSC melting endotherms were used to calculate the lamellar thickness distribution (LTD). In this approach, a DSC profile, heat flow versus temperature, is transformed into a lamellar thickness distribution (LTD) curve by using the Gibbs-Thomson equation expressed as in Eq. (1) [20]:

$$T_m = T_m^0 \left(1 - \frac{2\sigma_e}{\Delta H_f L} \right), \quad (1)$$

here $T_m^0 = 143.5^\circ\text{C}$ is the equilibrium melting temperature of crystalline lamellae of infinite thickness, $\sigma_e = 90 \text{ mJ/m}^2$ is the basal surface energy of the crystalline lamellae, $\Delta H_f = 290 \text{ J/cm}^3$ is the enthalpy of

fusion for the crystalline phase and L is the lamellar thickness (LT) of the samples melting at T_m [21].

Wide Angle X-ray Diffraction (WAXD)

The overall percent of crystallinity and crystallite sizes of the unaged and weathered PE samples were determined by WAXD. The X-ray measurements were carried out on a D8 Advance Power diffractometer (Bruker AXS GMBH, Germany) and performed at atmospheric pressure and at room temperature with a nickel-filtered Cu target K_α radiation ($\lambda = 0.154056$ nm) at 40 kV and 40 mA over a range of $2\theta = 10^\circ - 30^\circ$. The analyses of the spectra were carried out by means of the Eva 9.0 rev.0 software, Germany. The data were collected at a scanning rate of 6 deg/min with a step size of 0.02° .

The mathematical peaks deconvolution of the WAXD data were conducted by means of the Origin Pro 9 software. The overall crystallinity was calculated from the ratio of the total crystalline peaks areas A_{cr} and the total scattering peaks including the contribution of the amorphous phase ($A_{cr} + A_{am}$) using the following equation [22]:

$$X_C(\%) = \frac{A_{cr}}{A_{cr} + A_{am}} \times 100. \quad (2)$$

Field Emission Scanning Electron Microscopy (FESEM)

Samples with three hours of etching were examined with a FESEM microscope (Zeiss Supra 55 VP, Germany). The etching protocol was done in two steps followed by a washing cycle. Each step took one hour. The first etchant contained 0.7% wt/v of $KMnO_4$ dissolved in a mixture of concentrated H_2SO_4 and H_3PO_4 in proportion of 2 : 1. The second etchant contained 1% wt/v of $KMnO_4$ dissolved in a mixture of concentrated H_2SO_4 , H_3PO_4 and H_2O in proportion of 10 : 4 : 1.

The washing cycle following the etching began with a frozen mixture of H_2SO_4 and H_2O in the proportion 2 : 7, for 20 minutes, followed by a H_2O_2 (30%) rinsing for 20 minutes at room temperature. Then the samples were washed in distilled water for 5 minutes at room temperature. Finally, they were placed in acetone at room temperature for 20 minutes and then dried by compressed air. This etching procedure removed the detached impurities (degraded material) accentuating the reliefs and revealing the outer film surfaces [23].

The samples were immersed in liquid nitrogen and then cryofractured in shear to allow FESEM observation of both the etched and cryofractured surfaces. The energy of the electron beam was 20 kV, and the micrographs were obtained at a magnification of $1000\times$ for the cryofractured surfaces and from 1000 to $5000\times$ for cross-sections.

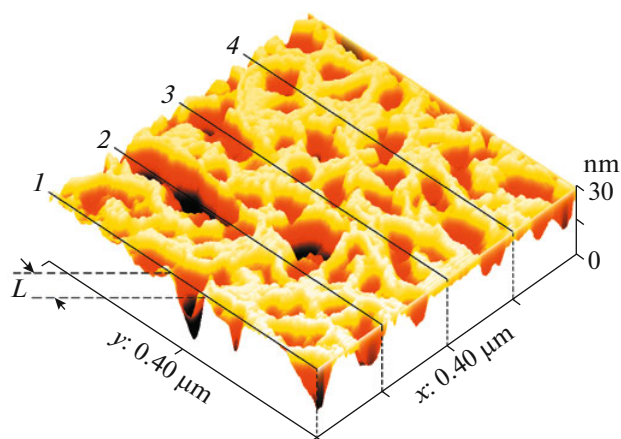


Fig. 1. (Color online) Typical 3D surface topography of LDPE films.

Atomic Force Microscopy (AFM)

The surface morphology of the treated specimens (etched) was studied using a Nano Navi (E-sweep) Universal Scanning Probe Microscope (USPM). The 3D surface morphology observations were conducted in the tapping mode with a constant force of 20 N/m and a resonance frequency of 0.15 kHz. From the analysis of the images the root-mean-squared roughness R_{rms} , the peak pitch (the maximum peak to valley height R_p) and the average roughness R_a for the topographic profiles, measured on $0.4 \times 0.4 \mu m^2$ images, were evaluated.

Furthermore, to quantify the evolution of the topographic peaks position against ageing in one direction (named X), the images were processed as follows. A measure of etched voids diameters where “ L ” is the diameter of the void in the Y direction and n is the number of voids along the selected Y positions. The average of voids diameters (named \bar{d}) for the image in the X direction and for four different equidistant positions in the Y direction allowed calculating their average values \bar{d} and that for each ageing time (Fig. 1), where

$$\bar{d} = \frac{\sum_{L=0}^n L}{n}. \quad (3)$$

RESULTS AND DISCUSSION

Ageing Effects on the Thermal Behavior

Figure 2 displays the heating and cooling DSC curves of the unaged and weathered LDPE films. The total heat of fusion (peak area in Fig. 2a) and that of re-crystallization (Fig. 2b) slightly increased with ageing. It is particularly important to notice that the crystallinity obtained initially was partially restored after ageing during the cooling process (Table 1). Indeed, it

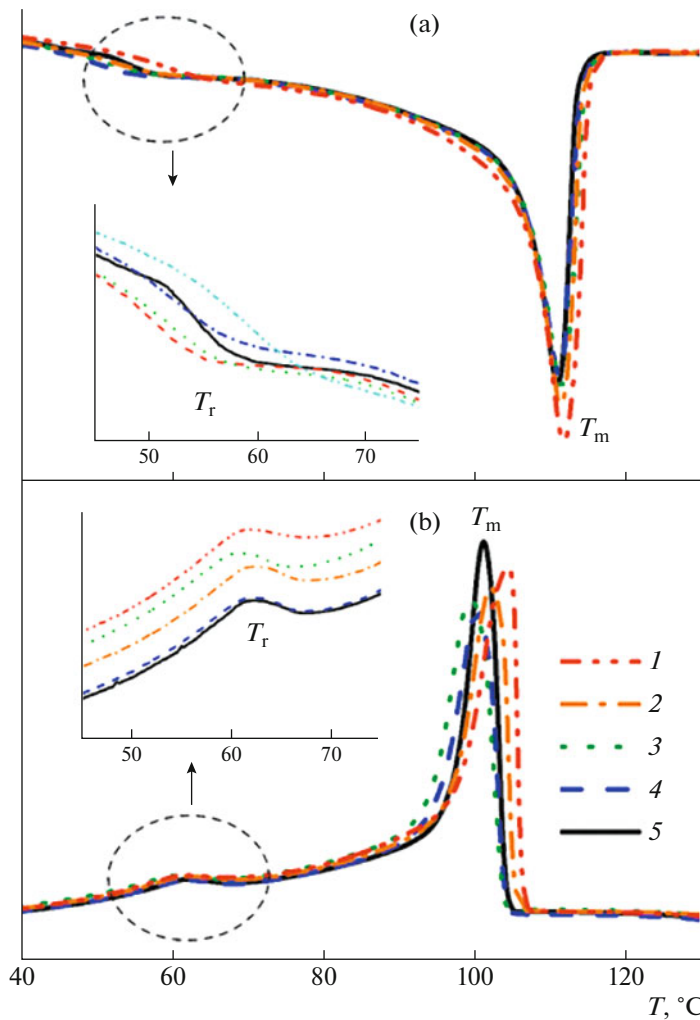


Fig. 2. (Color online) DSC (a) heating and (b) cooling curves of LDPE films (1) before and after (2) 2, (3) 4, (4) 6 and (5) 8 months of exposure.

was expected that, after melting, the prior crystallinity history would have been completely lost and the re-crystallization of the aged sample might have resulted in a small peak, very similar to that of the unexposed sample. The most interesting aspect in the cooling process is the reappearance of the two transitions but at higher temperatures for T_r (excepted for the last ageing stage) and lower temperatures for T_c . This means that despite the melting of all the crystallites during the heating process, the material, whatever its ageing stage was, it roughly recovered its initial morphology during cooling but different lamellar thicknesses (LT).

A comparative approach and an accurate analysis of the changing thermal properties of the material showed the impact of ageing on the material morphology. First of all, the melting temperature occurred around 111°C and increased very slightly with exposure. A transition temperature T_r , appearing only as a very weak shoulder around 54°C, became more visible with ageing and shifted slightly higher for 6 months

ageing (57.6°C) and then jumped to 65°C for 8 months ageing (Table 1).

According to Pabiot et al. the presence of several peaks represents the melting of lamellae of different sizes [24]. During heating the local melting of the smallest thicknesses occurs before the ones of thickest sizes. However, we found after a first heating-cooling cycle between -150°C and $+150^{\circ}\text{C}$, when a second scan was done in almost all the cases this low temperature transition disappeared [11]. The melting peak area increased with ageing time and a calculation of the crystallinity shows that it went from 39.5 to 51.9% meaning an increase of almost 34% due to the ageing. The same comparison for the cooling process showed that the difference between the initial sample re-crystallization and that of the most aged one was about 20.6%. This difference, we suggest, could be explained by the fact that, when melting the sample, a partial recombination of the damaged molecular chains could occur increasing the average molecular weight. This

Table 1. Transition temperatures of first order T_m , and of second order T_r , degree of crystallinity X_c , crystallization temperature T_c and specific heat C_p for unaged and aged LDPE films

Ageing, months	Heating				Cooling			
	T_m , °C	T_r , °C	X_c , %	C_p , J/(g K)	T_m , °C	T_r , °C	X_c , %	C_p , J/(g K)
0	110.9	54.2	39.5	0.29	101.1	62.2	35.9	0.26
2	111.1	54.6	40.9	0.29	100.3	62.1	35.7	0.26
4	111.4	55.5	43.3	0.31	101.2	62.1	35.7	0.27
6	111.3	57.6	44.7	0.32	101.8	62.1	38.8	0.28
8	111.7	65.3	51.9	0.38	104.4	61.7	43.3	0.31

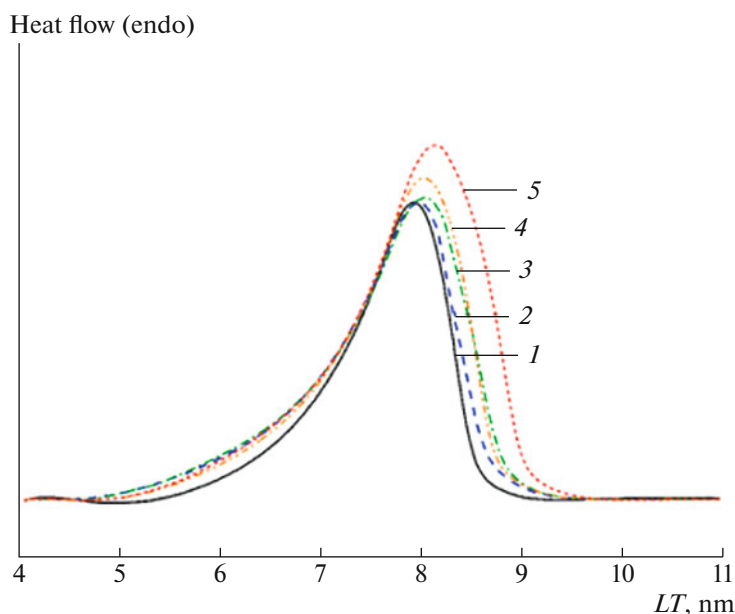
made it more difficult for the material to recover its original crystallinity degree gained by chain scissions during the ageing process. Indeed, longer macromolecules decrease the chain mobility which favors the secondary crystallization which we have called the chemo-crystallization process [11].

Figure 3 reports the lamellar thickness distribution (LTD) determined by the Gibbs Thomson equation (Eq. (1)) as applied to the DSC melting peaks data. From a statistical point of view each point of the curve corresponds to a lamellar thickness (LT) population, with the highest population corresponding to the maximum of the curve (i.e. the melting temperature T_m). With the ageing there was a slight increase in the intensity of the maxima of the curves accompanied by a broadening. The right side of the peak shifted towards higher lamellar thickness (LT) values while the height of the left side of the peak increased slightly and equally for all ageing times. In fact, the maximum of the peak went from 7.93 nm for the unaged sample up

to 8.13 nm for the most aged, and the largest lamellar thickness (LT), determined at the end of the peak where the curve meets the baseline went from 9.01 up to 9.49 nm. From these results it can be deduced that the short chain segments coming from the chains scission process due to ageing, promoted further the thickening of the existing lamellae by their diffusion toward the existing crystallites as the nucleation of new small ones. Both effects were responsible for the global increase of the crystallinity suggested to be due to either the incident solar energy absorbed by the film or by warming due to temperature, with increase in the crystallinity degree being higher for the last two months of the protocol which were the hottest times of the total exposure.

Crystal Structure and Unit Cell Parameters

The WAXD patterns of the LDPE films for different ageing stages are shown in Fig. 4. All the samples

**Fig. 3.** (Color online) Lamellar thickness distribution curves for unaged and weathered LDPE films (1) before and after (2) 2, (3) 4, (4) 6 and (5) 8 months of exposure.

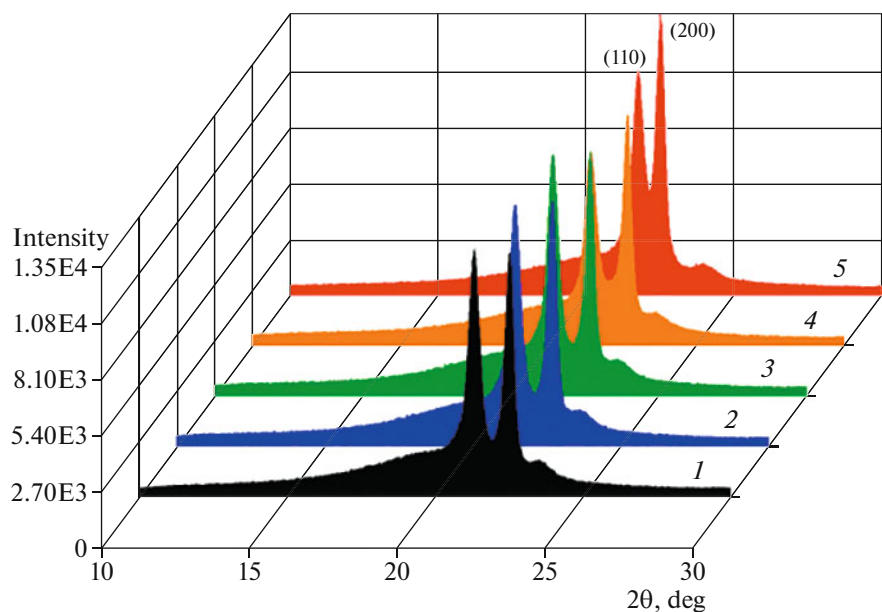


Fig. 4. (Color online) The WAXD patterns of LDPE films (1) before and after (2) 2, (3) 4, (4) 6, and (5) 8 months of exposure.

showed two large distinguishable reflection peaks (110) and (200) at 21.29° and 22.52° respectively, corresponding to the crystallographic planes of the orthorhombic lattice of polyethylene. The diffraction curves are combinations of an amorphous halo and crystalline peaks, specific to semi-crystalline polymers. The deconvolution of the peaks and the calculation of their respective areas allow determining the relative contribution of the crystalline peaks and the amorphous bump (amorphous “halo”) which permit calculation of the degree of crystallinity. As shown in the figure a slight increase of the peak areas and their respective maxima occurred.

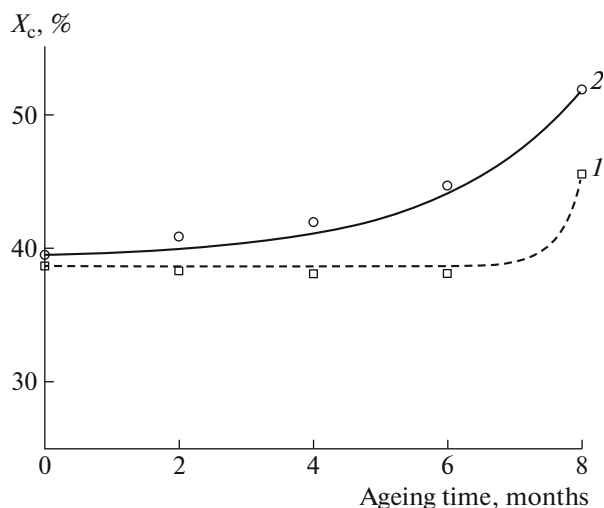


Fig. 5. Evolution of the crystallinity X_c of the LDPE films during climatic ageing. (1) XRD, (2) DSC.

The crystallinity was also calculated using the WAXD data as well as that in the DSC scans described above, of the WXR and, with the latter based on the area of the melting peak (Eq. (2)) [25]. The crystallinities function to ageing time measured by the two methods were expected to be different because of the different physical principles on which the two techniques are based; the crystallinity values recorded by the WAXD method (Fig. 5) were a little bit lower than those by DSC. For WAXD, the crystallinity (39% for unaged film) tended to remain constant till the sixth month, and then there was a significant increase for the last stage of ageing (to 45% at 8 months of exposure). For DSC, the crystallinity increased progressively to the last month of exposure.

The unit cell parameters and full width at half maximum (FWHM) as determined from WAXD scans are reported in Table 2. The crystalline peaks of the (110) and (200) planes of the unaged film had d -spacing of 4.2 and 4.0 Å, respectively. The values of the FWHM, generally associated with the internal strains, crystallite size and/or the perfection of the polyethylene crystallites, changed with ageing. If we analyze and compare separately the FWHM and the d -spacing of each crystallographic plane it appears that they varied differently. The widths of (110) plane diffraction peak became larger, except for the 4 months ageing and its d -spacing decreased (its peak position shifted to higher values) with increased exposure time. On the other hand, the width of the (200) plane diffraction and its d -spacing (peak position) did not change significantly.

We suggest that the facts that the 110 and 200 crystallographic planes became closer accompanied by the

Table 2. Unit cell parameters of LDPE films for different ageing stages

Ageing, months	(110)			(200)		
	2 θ	<i>d</i> -spacing, Å	FWHM, degrees	2 θ	<i>d</i> -spacing, Å	FWHM, degrees
0	21.2	4.2	0.47	22.5	3.95	0.37
2	21.3	4.2	0.48	22.6	3.93	0.37
4	21.4	4.2	0.46	22.7	3.92	0.35
6	21.4	4.1	0.52	22.7	3.92	0.37
8	21.8	4.1	0.53	22.6	3.95	0.36

broadening of the 110 peaks argue in favor the increase of crystallinity despite the crystallites' imperfection (different sizes). Therefore, ageing seems to reduce the internal strain because of the progressive chain rearrangement combined with the relaxation of the internal stress acquired during the film processing [26, 27].

LDPE Morphologies

Figures 6 show the FESEM surfaces morphologies of the unaged and naturally weathered samples. The surface of the control sample was found to be smooth, with fine granular particles (Fig. 6a). After 4 and 8 months (Figs. 6b, 6c), the concentration of these particles increased. This could be explained by the presence of the fine sand particles retained on the outer film surface, their concentration increase is related to the exposure duration of the material. Indeed, the FESEM images of the cryo-fractured cross-sections of the unaged (Figs. 7a–7c) and aged films (Figs. 7d–7i) revealed two distinguishable areas with different types of failure processes. Their respective surfaces displayed two zones (Figs. 7a, 7d, and 7g); one looked flat and uniform while the other contained similar grooves and crazes, more visible at higher magnifications (Figs. 7b, 7c, 7e, 7f, 7h, and 7i). The presence of the grooves very probably corresponds to the effect of tearing just after the crack propagation through the thickness. As a matter of fact, the bright streaks indicated the presence of crazes. For unaged samples, the grooves and crazes formed a layer in the vicinity of the external surface. This mode of failure is relevant to the viscoelastic character of the film before ageing. After four months of exposure, the grooves as well as the crazes multiplied and propagate in a greater thickness of the film (Figs. 7e, 7f). This phenomenon is explained by the fact that where the material is degraded it loses a part of its ductility (i.e. less crazes) and the failure was accompanied by more damages. In the last stage of exposure (Figs. 7h, 7i), this failure initiation mechanism multiplies where the material was more oxidized and crystallized, displaying smaller but numerous crazes in a smaller tearing zone, and the flat and uniform zone became larger, this is due to the brittleness of the material promoting the crack propagation with less tearing.

The AFM 2D pictures and the roughness profiles which highlight the surface topography of the unaged and weathered LDPE films are shown in Fig. 8. A cursory observation of the roughness profiles indicates an increase in the number of voids and the valley depth with ageing. The 3D representation of the aged samples supports the previous observation and reveals significant changes of the films surface (Fig. 9).

Table 3 lists the roughness parameters determined by analysis of the topography scans of the sample's surfaces. The surface profile parameters include average roughness R_a , the root-mean-squared roughness R_{rms} and the maximum peak to valley height R_t , for the different exposure times. The obtained results illustrate that the variations of the average roughness values R_a and maximum peak to valley height R_t values have the same trend as the variations of RMS roughness R_{rms} values; they all tend to globally increase except the R_t value of 6 months ageing and R_a value of 8 aged months.

To make more evident the effect of ageing on the sharpness and the increasing density of the peaks on the film surface, the variations of the peaks-spacing \bar{d} and the R_{rms} are presented function to ageing time (Fig. 10). It can be observed that \bar{d} decreased progressively and almost linearly with exposure time t , while R_{rms} increased linearly as well. This seems reasonable since these two parameters are logically inversely related.

Peaks-spacing follows a regression line which can be expressed by a mathematical equation ($-6.49t + 90.04$), that was applicable for the whole range of the exposure time (0–8 months). The same thing was

Table 3. Roughness parameters of LDPE films for different ageing time

Exposure time, months	R_{rms} , nm	R_t , nm	R_a , nm
0	3.57	14.69	2.78
4	4.42	18.57	3.54
6	4.73	15.15	3.69
7	5.26	23.91	3.13

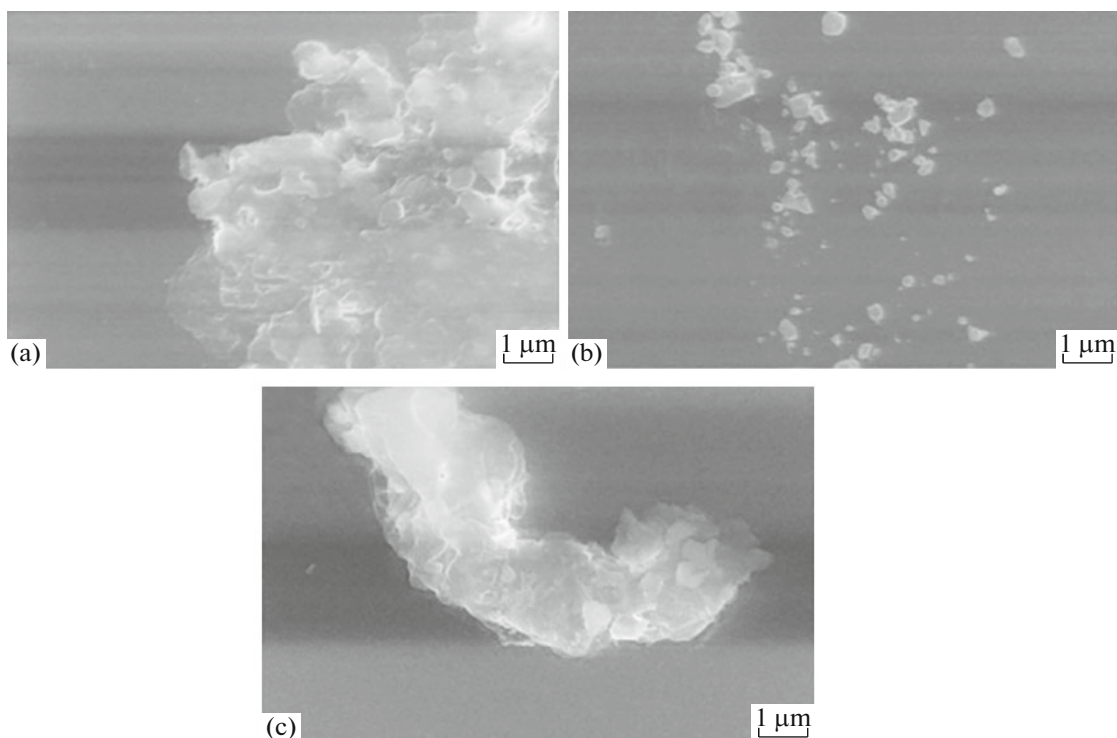


Fig. 6. FESEM images showing the surfaces morphologies of the LDPE films: (a) unweathered, (b) 4 months, and (c) 8 months of exposure.

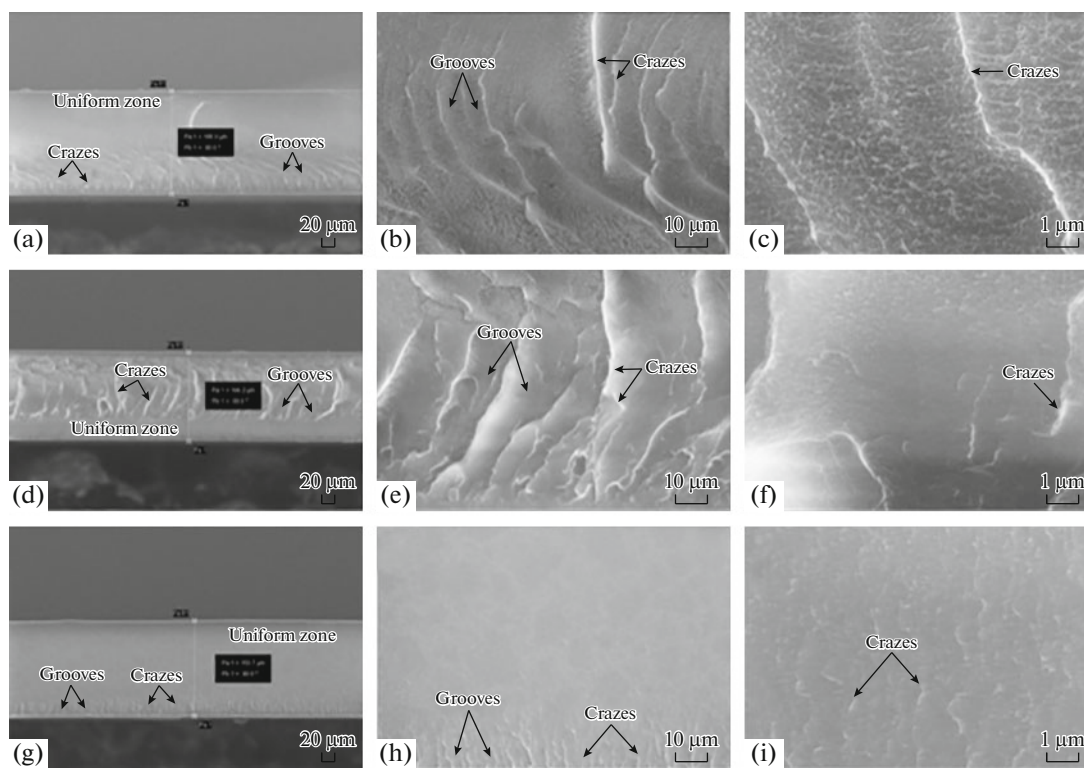


Fig. 7. FESEM images of the cryo-fractured cross-sections of the LDPE films: (a, b, c) unaged, (d, e, f) 4 months ageing, (g, h, i) 8 months ageing, each at various magnifications.

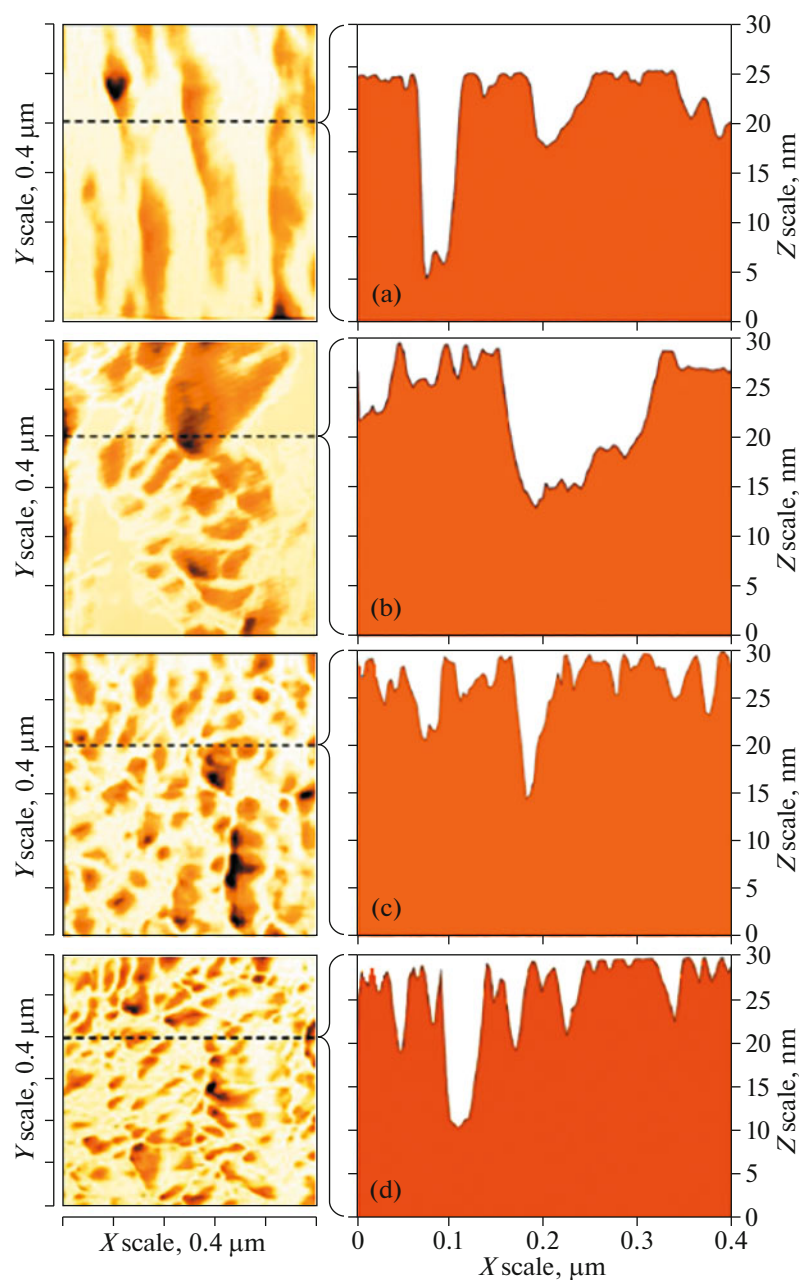


Fig. 8. (Color online) AFM 2D roughness profile of unweathered and weathered LDPE film surfaces for different exposure times: (a) unaged, (b) 2, (c) 6, and (d) 8 months aged.

observable for R_{rms} ($0.21t + 3.56$). The roughness and peak spacing varied inversely and both obeyed a mathematic law, thus demonstrating that they are linearly related to ageing time. These results also tie in with the FESEM observations discussed above.

These results demonstrated that ageing, which is a complex photo-oxidative process accompanied by morphological changes, significantly affected the surface topography of the films [7, 28]. La Mantian et al. have demonstrated that film ageing obeys to a gradient of chemical and physical defects along the thickness

[28]. As a matter of fact, after ageing the crystalline formation being more prominent at the outer film surface than in the core, this reduces the amorphous zones in favor of the crystalline ones. Therefore, this dramatically increases the surface roughness.

CONCLUSIONS

The present work showed that natural weathering leads to a rapid change of the morphological and surface properties of the LDPE studied film.

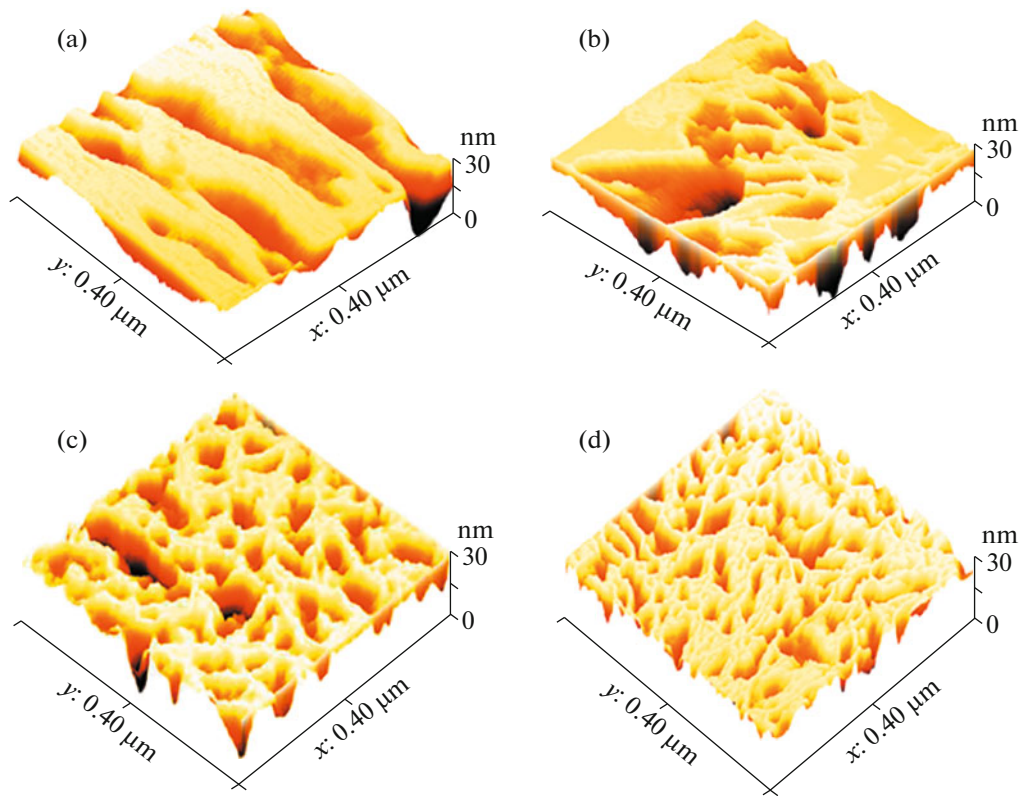


Fig. 9. (Color online) AFM 3D topographic representations of unweathered and weathered LDPE film surfaces for different exposure times; (a) 0, (b) 4, (c) 6, and (d) 8 months.

The complex photochemical mechanism taking place during ageing increases progressively the crystalline concentration by increasing either the lamellar thickness or by nucleating new crystallite.

These results corroborate with those of AFM which demonstrated that the film surface changes significantly with natural exposure. Indeed, the roughness and the height valley increase in reason of the increase of the surface crystalline zones. This result supports the hypothesis that the material degradation follows a gradient of physicochemical defects from the surface to the core through the film thickness. Interestingly, it has been found that the peaks-spacing and R_{rms} which logically progress inversely, followed an evolution that obeys to linear mathematical relationships.

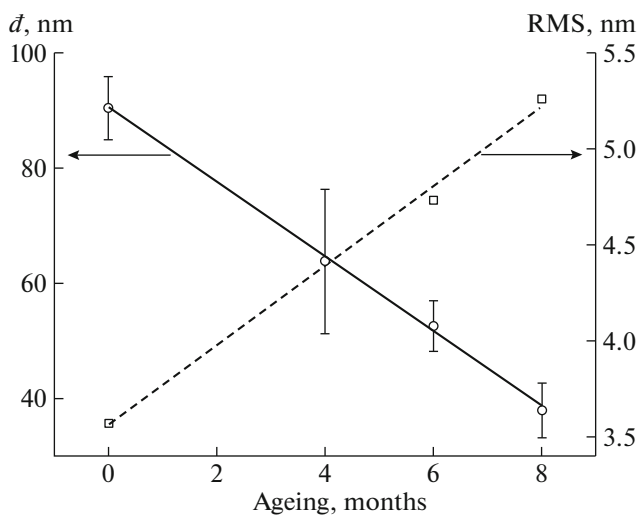


Fig. 10. Evolution of peaks-spacing \bar{d} and RMS with ageing.

FUNDING

The authors would like to acknowledge University of Teknologi Petronas (UTP), Malaysia, for the technical support during this study.

CONFLICT OF INTEREST

The authors declare that they have no conflicts of interest.

REFERENCES

1. M. Friedman and G. Walsh, *Polym. Eng. Sci.* **42**, 1756 (2002).

2. L. C. Mendes, E. S. Rufino, F. O. C. de Paula, and A. C. Torres, Jr., *Polym. Degrad. Stab.* **79**, 371 (2003).
3. C. C. Puig, C. Albano, E. Laredo, E. Quero, and A. Karam, *Nucl. Instrum. Methods Phys. Res., Sect. B* **268**, 1466 (2010).
4. S. D. Razumovskii and G. E. Zaikov, *Kinetics and Mechanism of Ozone Reactions with Organic Compounds* (Elsevier, Amsterdam, 1984), p.314.
5. S. N. Zhurkov, V. A. Zakrevskiy, V. E. Korsukov, and V. S. Kuksenko, *J. Polym. Sci., Part A: Polym. Chem.* **10**, 1509 (1972).
6. S. F. Chabira, M. Sebaa, and C. G'sell, *J. Appl. Polym. Sci.* **124**, 5200 (2012).
7. S. F. Chabira, M. Sebaa, and C. G'sell, *J. Appl. Polym. Sci.* **110**, 2516 (2008).
8. R. Singh, K. S. Samra, R. Kumar, and L. Singh, *Radiat. Phys. Chem.* **77**, 53 (2008).
9. A. Tidjani, *Polym. Degrad. Stab.* **68**, 465 (2000).
10. Y. Rui, Y. Jian, L. Ying, and W. Kunhua, *Polym. Degrad. Stab.* **88**, 333 (2005).
11. S. F. Chabira, M. Sebaa, R. Huchon, and B. De Jeso, *Polym. Degrad. Stab.* **91**, 1887 (2006).
12. M. I. Babaghayou, A. H. I. Mourad, V. Lorenzo, M. U. De la Orden, S. F. Chabira, and M. Sebaa, *Mater. Des.* **111**, 279 (2016).
13. T. Hirotsu, A. A. J. Ketelaars, and K. Nakayama, *Polym. Eng. Sci.* **40**, 2324 (2000).
14. M. R. Sanchis, V. Blanes, M. Blanes, D. Garcia, and R. Balart, *Eur. Polym. J.* **42**, 1558 (2006).
15. A. B. Ortiz-Magán, M. Mercedes Pastor-Blas, T. P. Ferrándiz-Gómez, C. Morant-Zacarés, and J. M. Martín-Martínez, *Plasmas Polym.* **6**, 81 (2001).
16. S. C. Park, S. K. Koh, and K. D. Pae, *Polym. Eng. Sci.* **38**, 1185 (1998).
17. B. M. Wickson and J. L. Brash, *Colloids Surf., A* **156**, 201 (1999).
18. U. Yilmazer, *J. Appl. Polym. Sci.* **42**, 2379 (1991).
19. F. J. Medel, F. Garcia-Álvarez, E. Gómez-Barrena, and J. A. Puértolas, *Polym. Degrad. Stab.* **88**, 435 (2005).
20. X. Huang, P. Jiang, C. Kim, J. Duan, and G. Wang, *J. Appl. Polym. Sci.* **107**, 2494 (2008).
21. H. Zhou and G. L. Wilkes, *Polymer* **38**, 5735 (1997).
22. Z. Mo and H. Zhang, *J. Macromol. Sci., Part C* **35**, 555 (1995).
23. H. B. H. Hamouda, M. Simoes-Betbeder, F. Grillon, P. Blouet, N. Billon, and R. Piques, *Polymer* **42**, 5425 (2001).
24. J. Pabiot and J. Verdu, *J. Appl. Polym. Sci.* **21**, 32 (1981).
25. M. Kaci and S. Cimmino, *Int. J. Polym. Anal. Charact.* **6**, 455 (2001).
26. A. V. Lyulin, D. Hudzinskyy, E. Janiaud, and A. Cha-teauminois, *J. Non-Cryst. Solids* **357**, 567 (2011).
27. A. Flores, F. Ania, and F. Baltá-Calleja, *Polymer* **50**, 729 (2009).
28. F. P. La Mantian and J. L. Gardette, *Polym. Degrad. Stab.* **75**, 1 (2002).